THE ASTROPHYSICAL JOURNAL, 335:468–485, 1988 December 1

ZODIACAL EMISSION. I. DUST NEAR THE EARTH'S ORBIT

WILLIAM T. REACH
Astronomy Department, University of California, Berkeley
Received 1988 March 31; accepted 1988 May 28

ABSTRACT

The infrared emission of interplanetary dust near the Earth's orbit is derived from *IRAS* observations of the gradient of in-ecliptic brightness tangent to the Earth's orbit, and the annual variation of the ecliptic polar brightness. Models with five grain constituents (graphite, magnetite, "astronomical silicate," andesite, and obsidian) and three size distributions (from Earth-orbiting satellites, lunar microcraters, and the coma of comet P/Halley) are compared with the observations. The observed emission is twice as bright as predicted; this discrepancy is due either to calibration errors or to enhanced radiative efficiency of "fluffy" particles. Graphite and magnetite particles are ruled out because they are too hot. The size distribution is constrained to be less steep than that derived from lunar microcrater studies, and is consistent with that obtained by Earth-orbiting satellites. Nonhomogeneous silicate grains with 3% graphite impurity produce the best fit to the spectrum. The model predictions extend from 3 μm to 1 mm, for use in analyzing future infrared background observations.

Subject headings: infrared: spectra — interplanetary medium — meteors and meteorites — zodiacal light

I. INTRODUCTION

The zodiacal emission (ZE) is the dominant background radiation in the mid-infrared. Work on the origin and physical properties of interplanetary dust has been largely based on optical observations of the zodiacal light (ZL), as is seen in recent conference proceedings (Giese and Lamy 1985; Halliday and McIntosh 1980). These observations have been made from ground-based observatories (e.g., Dumont and Levasseur-Regourd 1978) and from spacecraft (such as *Helios;* Lienert *et al.* 1981), and a general picture of the zodiacal dust cloud has developed. However, there are still major gaps in our understanding of interplanetary dust. In particular, the spectrum and polarimetry of the ZL reveal little about the grain composition other than constraints on the optical constants in the visible. Observation and analysis of the ZE are better suited to determining the composition of interplanetary dust.

In § II we calculate the spectrum of dust near the Earth's orbit, assuming spherical, homogeneous grains and a size distribution based on *in situ* measurements. Our calculations comprise an update of those of Röser and Staude (1978), who predicted the ZL and ZE using similar model assumptions. Frazier, Boucher, and Mueller (1987) have also made similar model calculations. The most important new feature of our calculations is the grain-size distribution: we used new size distributions obtained from Earth-orbiting satellites, the lunar microcrater distribution, and satellites participating the comet P/Halley rendezvous of 1986. We also use new optical constant data.

Recently, the ZE has been observed over the entire sky by the *Infrared Astronomical Satellite* (*IRAS*; Hauser *et al.* 1984). *IRAS* has greatly increased our observational knowledge of the ZE, by providing uniform data over an entire year of observation at relatively high angular resolution. Since the observed brightness in a given direction is produced by all of the dust along the line of sight, it is not straightforward to interpret the ZE spectrum without introducing a model for the dust density as a function of position in the solar system. In § III we use two different methods to determine the spectrum of dust near the Earth's orbit, using *differential* measurements of the ZE brightness which make integration along the line of sight unnecessary.

Previous ZE observations (e.g., Murdock and Price 1985; Briotta 1976) were more limited in scope, but the general shape of the zodiacal dust cloud and ZE spectrum were already known. However, the total brightness of the ZE observed by each instrument is different; the ZE brightness observed by Murdock and Price (1985) is fainter than that observed by *IRAS* by a factor of about 2. The spectrum of the ZE is much more consistent from instrument to instrument (Salama *et al.* 1987). Until the absolute calibration of the ZE brightness is independently determined by well-calibrated observations, we are forced (in § IV) to rely on the spectral shape in constraining the dust constituent.

II. PREDICTION OF THE INFRARED EMISSIVITY

a) Theory

The ZE is thermal reemission of energy absorbed from sunlight by dust in the interplanetary medium. We assume here spherical, homogeneous particles, so a grain is fully specified by its radius, a, and constituent material. The temperature of a grain is determined by radiative equilibrium:

$$\int F_\nu^\odot Q_{\rm abs}^{(i)}(a, \nu)d\nu = \int B_\nu(T^{(i)}(a))Q_{\rm abs}^{(i)}(a, \nu)d\nu \, . \qquad (1)$$

In this equation $F_\nu^\odot$ is the solar flux (taken from Allen 1973); $Q_{\rm abs}^{(i)}$ is the absorption cross section, in units of the geometric cross section, for particles composed of constituent material i; and $B_\nu(T)$ is the Planck function evaluated at the grain temperature T. Equation (1) may be rewritten in a more transparent form,

$$T = 278 \text{ K}[\bar{Q}_\odot/\bar{Q}(T)]^{1/4}d^{-1/2} \, , \qquad (2)$$

where $\bar{Q}_\odot$ is the absorption efficiency averaged over the solar spectrum, $\bar{Q}(T)$ is the absorption efficiency averaged over a blackbody spectrum at temperature T, and d is the distance from the grain to the Sun in AU. This equation must be solved by iteration, since the temperature dependence of $\bar{Q}$ is complicated.

Throughout this paper, the term *emissivity* and the symbol $\mathscr{E}_\nu$ are defined in the sense of radiative transfer theory, in such a way that the brightness of the ZE is the integral of the emissivity over the path defined by the line of sight (cf. Lang 1980, p. 27). Another frequently used definition of emissivity (cf. Bohren and Huffman 1983, § 4.7) is, in the notation used in this paper, $\bar{Q}(T)$.

Given the temperatures, the volume emissivity of an ensemble of particles is calculated by integrating over the size distribution and summing over the constituents:

$$\mathscr{E}_\nu = \sum_i \int da \, \frac{dn^{(i)}}{da} B_\nu(T^{(i)}(a)) Q^{(i)}_{\rm abs}(a, \nu) \, . \quad (3)$$

The size distribution is expressed in terms of the quantity $(dn^{(i)}/da)da$, the number density of particles composed of material i with radius between a and $a + da$. In principle, the size distribution for particles of different composition can be different; however, we shall assume for simplicity that the size distribution has the same dependence on radius for particles of all compositions. The limits of integration in equation (3) are important for some choices of the particle size distribution. In particular, the smallest particles dominate if the size distribution is steeper than approximately a^{-3}. For the size distributions considered in this paper, the integrand in equation (3) becomes negligible by the small-particle cutoff of 50 Å radius, as is shown below (§ II *d*[*i*]).

b) Optical Properties of the Grains

i) *Grain Constituents and Optical Constants*

Various materials have been suggested as the constituents of interplanetary dust. In order to include a particular constituent in our calculations, the index of refraction must be known from a wavelength of 1600 Å (from the solar spectrum) to approximately 100 μm. (The upper limit depends on the grain temperature. For the present calculation no optical data longward of 100 μm were needed, but for cooler grains, such as exist in the outer solar system and interstellar medium, optical data at even longer wavelengths are needed.) We are thus restricted to a small selection of materials. It may become possible soon to measure the optical constants of stratospheric interplanetary dust particles directly (S. Sandford 1988, private communication), after which the calculations described in this paper should be repeated with the new optical data.

1. *Carbonaceous material.*—The only constituent for which a strong argument can be formed based on *a priori* considerations is carbonaceous material, since C is abundant in interstellar space and is predicted to form solids in stellar outflows. Direct evidence for carbonaceous material as a major constituent of cometary dust was obtained by the mass spectrometers aboard *Giotto* (PIA) and *Vega-2* (PUMA) during the P/Halley rendezvous of 1986. These mass spectrometers measured the elemental abundances for individual grains. While the abundances for most elements were nearly identical with those of chondritic material, the abundance of C in the dust was found to be in excess by a factor of ~8 (Langevin *et al.* 1987 [*Vega-2*]; Clark, Mason, and Kissel 1987 [*Giotto*]). The excess carbonaceous material, referred to as "CHON" (carbon-hydrogen-oxygen-nitrogen–rich) is apparently contained in a population of grains separate from the silicate material (discussed below), as evidenced by the lack of correlation of C and Si abundance in the dust samples (Langevin *et al.* 1987).

The optical properties of carbonaceous material depend strongly on the conditions under which they are formed. The three main classes of carbonaceous material are graphite, diamond, and amorphous carbon. Graphite is a layered solid, with the C atoms arranged in planes and the bonding (called sp^2) most strong within the planes. A large energy gap provides graphite with a large density of conduction electrons, so graphite behaves like a metal. (This property also makes the dielectric function of graphite temperature-dependent.) Carbon can also form a diamond lattice, with tetrahedral bonding (called sp^3) between the C atoms. Recently, sp^3 domains with diamond lattice structure have been discovered in meteorites (Lewis *et al.* 1987). Finally, amorphous carbon has sp^3 bonding, like diamond, but without long-range order. The amount of amorphous carbon in interplanetary grains is difficult to assess.

We use the optical properties of graphite as representative of carbonaceous material. The optical properties of amorphous carbon have been measured in the visible and near-ultraviolet (e.g., Colangeli *et al.* 1986), and the results are qualitatively similar to those for graphite. Experimental measurements of the optical properties of amorphous carbon in the infrared are not fully consistent with one another. Only for graphite are the optical constants known from the far-infrared to the near-ultraviolet. Our absorption curve for 0.1 μm radius graphite spheres is very similar to that used for amorphous carbon by Martin and Rogers (1987), and our extinction curve for 0.01 μm graphite spheres is very similar to the amorphous carbon extinction curve measured from the visible to the infrared by Bussoletti, Colangeli, and Orofino (1987). Diamonds are presumably only a small fraction of the total grain mass. It is possible that small diamonds, unincorporated into larger grains, exist in the interplanetary medium; such a separate grain population is neglected in our calculations.

The graphite index of refraction was calculated from the dielectric function presented by Draine and Lee (1984, hereafter DL). The optical data on which DL based their calculations were taken mainly from reflectance measurements of graphite samples cleaved parallel to the graphitic planes (Taft and Phillip 1965; Phillip 1977). Graphite is a highly anisotropic material, so its optical properties for radiation incident perpendicular to the graphitic planes are totally different. As in DL, the dielectric function of a graphite grain was calculated by combining the dielectric function for normal and perpendicular incidence with multiplicative factors $\frac{1}{3}$ and $\frac{2}{3}$, respectively, as would be appropriate for randomly oriented grains. (It is not clear whether the calculations described in § II*b*[ii], which are based on spherical grains, are valid for an anisotropic dielectric function; however, the theory has been proved to be correct in the small-particle limit [cf. Bohren and Huffman 1983].) The temperature dependence of the dielectric function is based on laboratory data (see DL) and is significant for the range of temperatures considered in this paper. Finally, the effect of finite particle size on the dielectric function was modeled theoretically as an increased electron collision rate within smaller particles (DL).

2. *Silicate material.*—The arguments for the existence of silicate particles in the interplanetary medium are all empirical and therefore even more compelling than the arguments for carbonaceous material. Terrestrial and lunar rocks and stony meteorites are composed largely of silicates. Mass spectrometers aboard spacecraft participating in the P/Halley flyby measured abundances in general agreement with the abundances of chondritic meteorite material, but with Mg some-

what enhanced (Langevin *et al.* 1987). These observations demonstrate that cometary silicates are Mg-rich, and two-thirds of all grain minerals consist of Mg-rich silicates (Langevin *et al.* 1987). Furthermore, infrared spectra of interplanetary dust particles collected in the stratosphere have strong 10 μm features (Sandford and Walker 1985), which are the hallmark of silicates.

The dielectric properties of silicates share some common features, including the presence of spectral features near 10 and 20 μm, but they also show considerable variance. The 10 μm features are due to Si-O stretching vibrations, and the 20 μm features are due to Si-O-Si stretching vibrations; these features are present in all silicates due to the SiO_4 group which is their defining chemical characteristic. On the other hand, the opacity of different silicate minerals at visible wavelengths spans 2 orders of magnitude, while the infrared properties are relatively consistent from particle to particle.

We used the dielectric functions for andesite and obsidian[1] (Pollack, Toon, and Khare 1973), and the dielectric function created by DL, called "astronomical silicate." The astronomical silicate data are actually a combination of laboratory data for olivine at high photon energies and astronomical observations of the Trapezium and oxygen-rich M star outflows in the infrared. The resulting dielectric function is similar to that obtained from laboratry measurements of olivine smoke (Huffman and Stapp 1973), but with a ratio of infrared to visible opacity which is substantially larger. While the astronomical silicate dielectric function does not correspond to any known material, it is a useful representation of the properties of "dirty" silicates. (As shown below in § IV, real silicates with graphite impurities closely resemble astronomical silicate.) In order of increasing visible opacity, the silicates used in this paper are obsidian, andesite, and astronomical silicate.

3. *Other materials.*—For comparison with the results for graphite and silicates, we have also performed our calculations for magnetite (Fe_3O_4). Magnetite was considered a plausible constituent of interstellar dust in order to explain the strong polarization of starlight and perhaps the diffuse interstellar bands. Its presence as a major constituent of interstellar and interplanetary dust is doubtful, however, because the cosmic abundance of Fe is low. Magnetite is certainly present in meteorites, some of which are composed (by mass) largely of Fe. The most distinctive features of magnetite in the infrared are two strong absorption bands at 20 and 30 μm. The magnetite features are carried into the predicted ZE spectrum in a manner different from that for the silicate features; magnetite is an example of a material which produce net *absorption* in the ZE. The index of refraction of magnetite was taken from Huffman (1977).

A final index of refraction which is useful for illustration is a constant over all wavelengths. The interplanetary dust constituent must be strongly absorbing; otherwise the observed ZE color temperature would not be near the temperature predicted for blackbody grains, as is observed (§ III). We thus chose $m = 1 - i$. This case will not be considered a possibility for the interplanetary dust, since a constant index of refraction from the visible to the infrared is not observed for any known material. We will refer to the hypothetical material with constant index of refraction as "constantite" in this paper.

There are other materials which should be included in our calculations. For many of these, the optical properties in the infrared are not known sufficiently accurately. Others are neglected, for the time being, simply to keep the total number of candidate material small. New materials discovered in interplanetary dust and meteorites will be incorporated as they are discovered and their optical properties are measured. For example, SiC grains were recently discovered in a meteorite (Bernatowicz *et al.* 1987). Finally, many types of nonhomogeneous particles, consisting of domains of two or more different minerals, are possible. Mixtures of silicates and graphitic impurities are treated in § IV, but clearly the total number of possibilities is large.

ii) *Calculation of Absorption Efficiencies*

1. *Method of calculation.*—The absorption efficiency, Q_{abs}, is defined in such a way that the cross section for absorption of a photon of wavelength λ by a spherical particle of radius a is $\pi a^2 Q_{abs}(a, \lambda)$. The theory necessary for the calculation of Q_{abs} (Mie theory) is described in the monographs of van de Hulst (1957), Kerker (1969), and Bohren and Huffman (1983), to whom we refer the reader for details. We note here only some practical details of the method of calculation. First, let us define the parameter $x = 2\pi a/\lambda$ and the index of refraction $m = n - ik$. For $x \ll 1$, the absorption efficiency may be expanded into a power series (e.g., van de Hulst 1957, § 14.21). An improved version of this series, which is more accurate than the van de Hulst series when $k \ll 1$, is given by Wiscombe (1980); we used this series for $|m|x < 0.01$.

For intermediate x, the Mie coefficients must be calculated and the absorption efficiency formed from summations (van de Hulst 1957, §§ 9.22 and 9.32). The summation must be carried out to terms which involve Bessel functions of order $n_{max} = x + 4x^{1/3} + 2$ (Wiscombe 1980). Because of numerical round-off errors, some of these Bessel functions cannot be calculated by standard forward recursion relations. (Any routine using only forward recurrence is limited to $x < 10$ for most indices of refraction.) In these cases, the recursion relations are calculated backward from the last value required. This last value is calculated by the continued-fraction method of Lentz (1976), which has high accuracy for terms of large order. Using the Lentz method and backward recurrence allows calculations up to $x = 10{,}000$ with no evidence for numerical errors.

2. *Resulting absorption efficiencies.*—Absorption curves for the materials described above were calculated from the near-ultraviolet to the far-infrared for the range of particle sizes (0.1–100 μm) that dominate the ZE (see § II*d*[i]). For illustration, the absorption curves of "astronomical silicate" grains are shown in Figure 1. Two properties of these curves deserve attention. First, the 10 and 20 μm spectral features are present as enhanced absorption for particles of radius 1 μm and smaller. The absorption curve of larger particles is dominated by the *real* part of the index of refraction, since these particles are optically thick both at the wavelength of the spectral feature and in the surrounding continuum. Thus if the particle-size distribution does not contain enough particles smaller than 1 μm, the 10 μm silicate feature will not be present in the spectrum.

Strong resonances, or "ripples," are present in Figure 1 for particles larger than 1 μm. The ripples exist only for dielectrics, which have small absorptivity; metallic particles of graphite and magnetite show no ripples. Although the ripples are smoothed out after integration over the size distribution and do not appear in the emission spectrum as fixed features, it is

[1] Of the two obsidian samples measured by Pollack, Toon, and Khare (1973), we used "Lake County, Oregon."

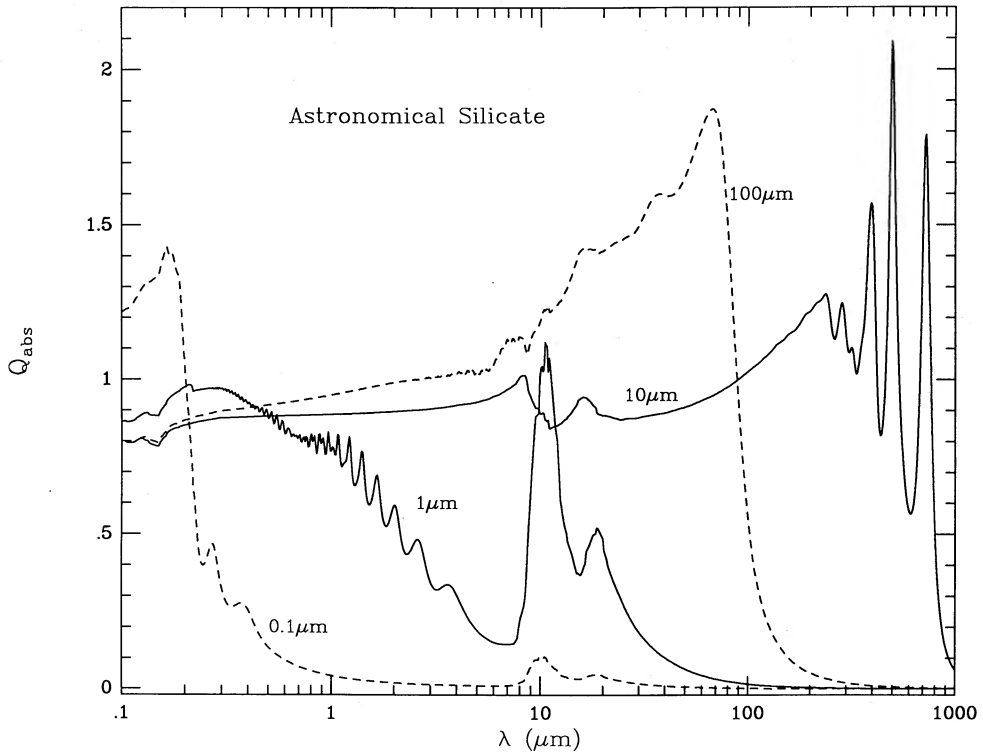

FIG. 1.—Absorption efficiency as a function of wavelength for spherical particles of "astronomical silicate." Curves are labeled by particle radius in microns.

important to treat them carefully. It is necessary to calculate the absorption efficiencies with a grid fine enough to resolve the resonances.

iii) *Grain Temperatures*

The temperatures, calculated from equation (2), for grains at 1 AU from the Sun are shown as a function of particle size in Figure 2. Consider first the simple case of "constantite" ($m = 1 - i$). Small particles are hotter than larger particles of "constantite" because their infrared absorption efficiency is lower. The temperature decreases as a function of (increasing) particle size until the blackbody temperature (278 K) is reached. The trend ends when the peak of the thermal emission passes out of the infrared. Large grains absorb and radiate like blackbodies. The smallest particles in Figure 2 ($a < 0.1$ μm) are in the Rayleigh limit in both the visible and the infrared; the ratio of infrared to visible aborption is thus independent of particle size, and a limiting temperature is reached. Graphite and magnetite both behave like constantite, except that the limiting temperatures for small particles are different (700 K for graphite, 600 K for magnetite).

Silicates, on the other hand, behave differently. Since they are nearly transparent in the visible but relatively opaque in the infrared, small silicate particles are even cooler than blackbody grains. Further, infrared emission features of silicates act as coolants. The limiting temperature for small particles is 170 K for andesite and 100 K for obsidian. These low values are due to the near-transparency at visible wavelengths of the glassy samples which Pollack, Toon, and Khare (1973) measured. The astronomical silicate temperatures are generally higher, with a limiting value of 285 K for small particles. The peculiar dependence of temperature on particle size for astronomical silicate is caused by the shape of the olivine refractive index which was used for high photon energies. It is evident that a range of temperatures is possible for small silicate particles, depending on the opacity at visible wavelengths. Note, however, that Pollack, Toon, and Khare (1973) measured large, pure mineral samples. It would be no surprise to find that interplanetary silicates contain impurities, such as carbonaceous material, and thus have higher visible opacity. (Models of silicate/graphite mixtures are discused in § IV.)

c) Size Distribution

Observations of the density and size distribution of interplanetary dust have been recently discussed by Grün *et al.* (1985). They derived the flux (particles m^{-2} s^{-1}) as a function of particle size from two data sets: one from the "beer can" type of particle detector aboard four satellites (*HEOS 2*, *Pioneer 8* and *9*, and *Pegasus*) and the other from the lunar microcrater distribution. Similar results were obtained for large particles ($a > 2$ μm), but the lunar microcrater data imply a substantially larger flux of submicron particles. The microcrater distribution is probably dominated by secondary cratering for pits smaller than 7 μm diameter (Zook *et al.* 1984), so the satellite results are to be preferred for smaller particles. Further, Grün *et al.* showed that the microcrater distribution is inconsistent with the color of the visible and ultraviolet zodiacal light; we reach a similar conclusion using the infrared data for some constituent materials. Considering the effect of collisional redistribution of particle sizes, Grün *et al.* calculated the distribution of particle sizes consistent with the satellite data ("interplanetary flux" see their eq. [A3]) and the microcrater data ("lunar flux"; their eq. [A2]). These size distributions are shown together in Figure 3.

Maurette *et al.* (1987) recently reported an independent measurement of the flux of interplanetary dust at the Earth's orbit. Particles discovered in ice samples from Greenland and

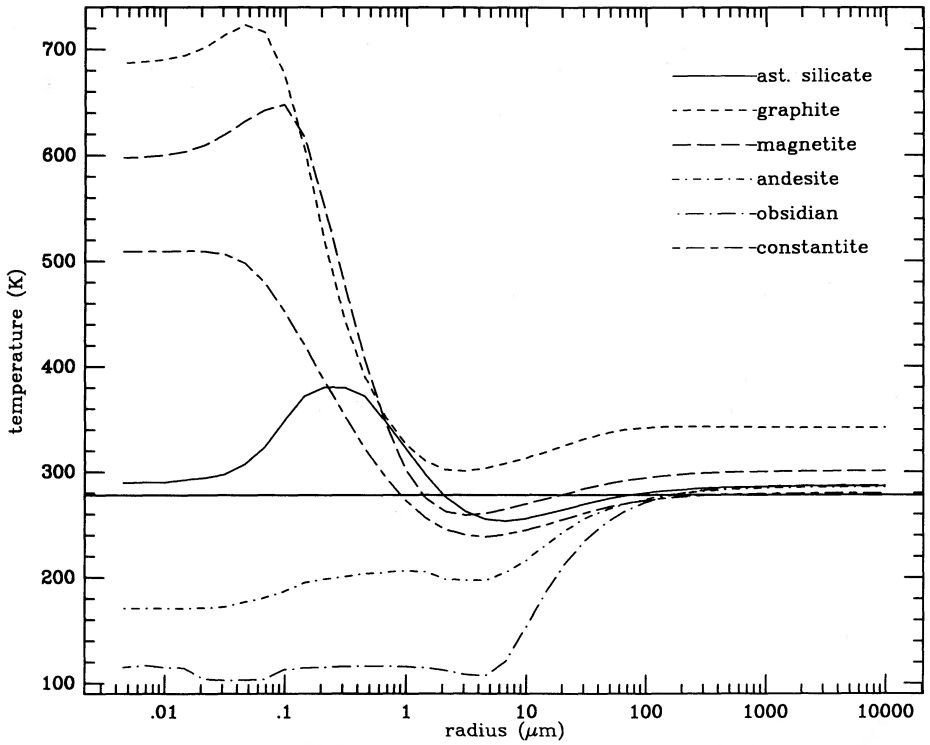

FIG. 2.—Temperature of spherical grains, illuminated by the solar flux at the Earth's orbit, as a function of particle size for the materials used in § II

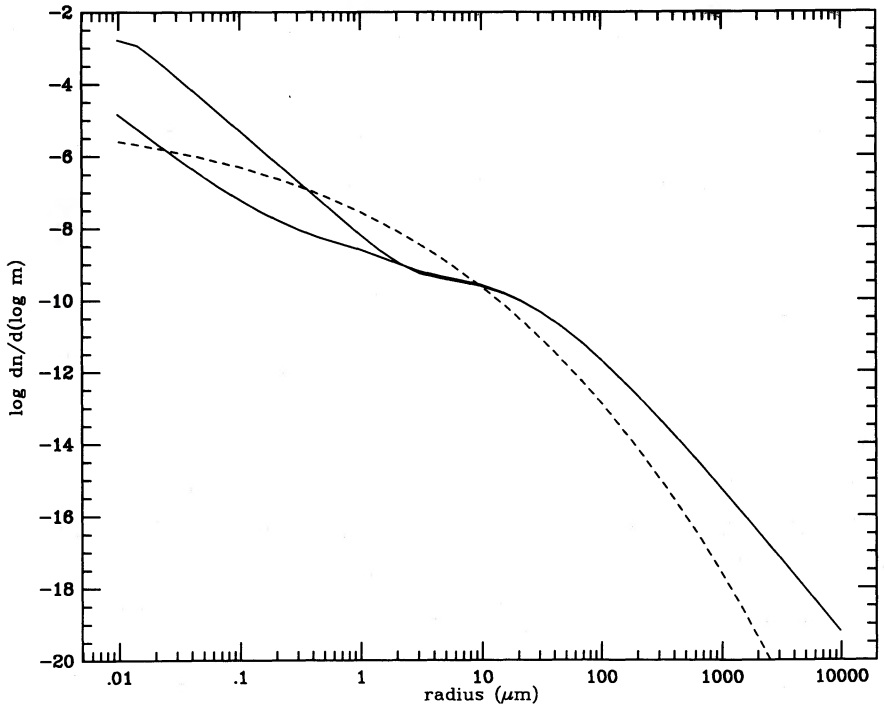

FIG. 3.—Differential particle-size distribution, as a function of particle radius, from Grün *et al.* (1985) (*solid curves*) and from the coma of comet P/Halley (*dashed curve*). The units are m^{-3} per logarithmic particle mass interval. (The grain density was assumed to be 2.5 g cm^{-3}.) Of the two Grün *et al.* models, the "lunar" model has a higher number density of particles smaller than 1 μm; above 1 μm, the "lunar" and "interplanetary" models are identical.

believed to be extraterrestrial (based on elemental abundance measurements) have a size distribution very similar to those of Grün *et al.* (1985). The particles studied in detail were large ($a > 50$ μm), so it is not possible to use the Greenland data to discriminate between the lunar and interplanetary models of Grün *et al.* Also, the degree of contamination of their sample by terrestrial particles, fragmentation, and melting residues is difficult to assess.

The best data on the size distribution of any cosmic dust were obtained by spacecraft during the comet P/Halley encounter of 1986. Impact detectors aboard the *Giotto* (DIDSY) and *Vega-2* spacecraft provided particle flux data within ~10 particle size bins as a function of time during passage through the coma (McDonnell *et al.* 1987; Mazets *et al.* 1986). The size distribution was observed to vary both regularly, with position in the coma, and irregularly, with the level of activity of the nucleus. For the purpose of this paper, the particle flux integrated over the encounter interval, the so-called fluence, was used. The differential number density distribution was derived from the fluence, using a simple r^{-2} density law in the coma, by Lamy, Grün, and Perrin (1987). The polynomial fit to their results was converted from units of particle mass into particle radius using a constant density of 2.5 g cm^{-3}. The size distribution is that of the cometary coma, clearly too dense for the interplanetary medium. Thus the normalization of the size distribution, to which we refer as "Halley" in this paper, is a free parameter. In Figure 3, and in the other figures in this paper, Halley size distribution is normalized to the interplanetary size distribution at a particle radius of 10 μm.

d) Calculation of the Emissivity

i) *Range of Important Particle Sizes*

In order to determine the range of particle sizes that dominate the ZE, we calculated and plotted the integrand of equation (3), to which we refer hereafter as the "emissivity integrand," as a function of particle size for several infrared wavelengths. Consider first Figure 4, which presents the emissivity integrand of "constantite" at wavelengths of 12, 25, and 60 μm for (*a*) the interplanetary and (*b*) the lunar size distribution models. The emissivity integrand shows a simple peak at $a \simeq 30$ μm for the interplanetary model at all wavelengths, and for the lunar model at all wavelengths except 12 μm. The lunar model at 12 μm shows an additional peak at particle radius $a \simeq 0.1$ μm. We may divide the particles into two distinct populations on the basis of this result: the "classical" particles produce the main peak and have radii between 1 and 200 μm; the "submicron" particles produce the excess 12 μm emission and have radii between 0.02 and 1 μm. The reason for the extra peak in the lunar model is that submicron grains are more abundant than in the interplanetary model. Submicron grains are hotter than the classical grains of constantite (see Fig. 2), so their thermal emission peaks at shorter wavelengths. At wavelengths longer than 12 μm, the classical population dominates; at shorter wavelengths, the submicron population becomes dominant. The emissivity integrands for graphite and magnetite reveal the same grain population effects as constantite.

The silicates obsidian and andesite do not produce substantial emission from the submicron population. Small particles of these materials are actually cooler than large particles, and the radiative cross section of the submicron population is too small to produce as much emission as the classical population does. There is no qualitative difference between the predictions of the lunar and interplanetary size distributions, since the two size distributions are identical for classical grains. The situation for astronomical silicate is somewhat different. The two grain populations are evident, with the submicron population producing substantial 12 μm emission for the lunar flux model. The emissivity integrand at 10 μm, the center of the olivine Si-O stretch spectral feature, is produced by both submicron and classical grains, with roughly equal contributions from each. Since the 10 μm feature is present in the absorption curves of submicron grains but not in those of classical grains (Fig. 1), this feature will appear in the spectrum for the lunar size distribution. There can be no spectral feature for the interplanetary model, because the classical population produces all the emission.

Now consider the range of particle sizes which dominate the ZE if the Halley size distribution is used. Rather than two distinct populations of grains, there is a gradual transition such that larger grains are responsible for the longer wavelength emission. The particle sizes which dominate the ZE at each wavelength satisfy $a = \lambda/2\pi$, or equivalently $x = 1$, for astronomical silicate, graphite, and magnetite. Since the size distribution is smooth and monotonically decreasing, the dominant particles are those which are just larger than the Rayleigh-Gans regime ($x \ll 1$). Andesite and obsidian are exceptions to this rule, since small particles are too cool to produce substantial emission. The dominant particle size is thus shifted up to $a = 20$, 20, and 40 μm for $\lambda = 12$, 25, and 60 μm, respectively.

ii) *Resulting Emission Spectra*

The emission spectrum predicted for each grain constituent is shown in Figure 5. Each panel shows the volume emissivity predicted if all grains responsible for the particle flux measurements described in § II*c* are composed of a single constituent.

The difference between the size distributions is very pronounced for graphite (Fig. 5*a*) and magnetite (Fig. 5*b*). The hot submicron grains dominate at wavelengths below 10 μm, producing a spectrum with a significantly high color temperature. The magnetite features are very deep for all size distributions, since they are carried by large particles; they would be easily detectable by observations with a resolution $\lambda/\Delta\lambda > 4$.

The silicate spectra are similar to each other in overall shape (continuum), since the emission is produced mostly by classical grains. These particle are at or near the blackbody temperature, so it is difficult to distinguish one type of silicate from another using only the color temperature of the emission spectrum. The color temperatures for our three silicate spectra are generally in agreement with the expectations based on the transparency of the sample materials (§ II*b*[i]2).

The 10 and 20 μm spectral features are very different for our three silicate and size distributions. For astronomical silicate (Fig. 5*c*) there is a difference between the spectra predicted by the lunar and the interplanetary size distributions: for the lunar model the 10 and 20 μm features are present in emission. The features are even stronger using the Halley size distribution. The 10 μm feature is superposed on the steep Wein portion of the continuum, but it may be observable with moderate spectral resolution instruments. (The 20 μm feature is more difficult, since it lies precisely at the peak of the continuum spectrum.) The predicted spectrum for andesite (Fig. 5*d*) is practically featureless, and there is no difference between the lunar and interplanetary size distributions.

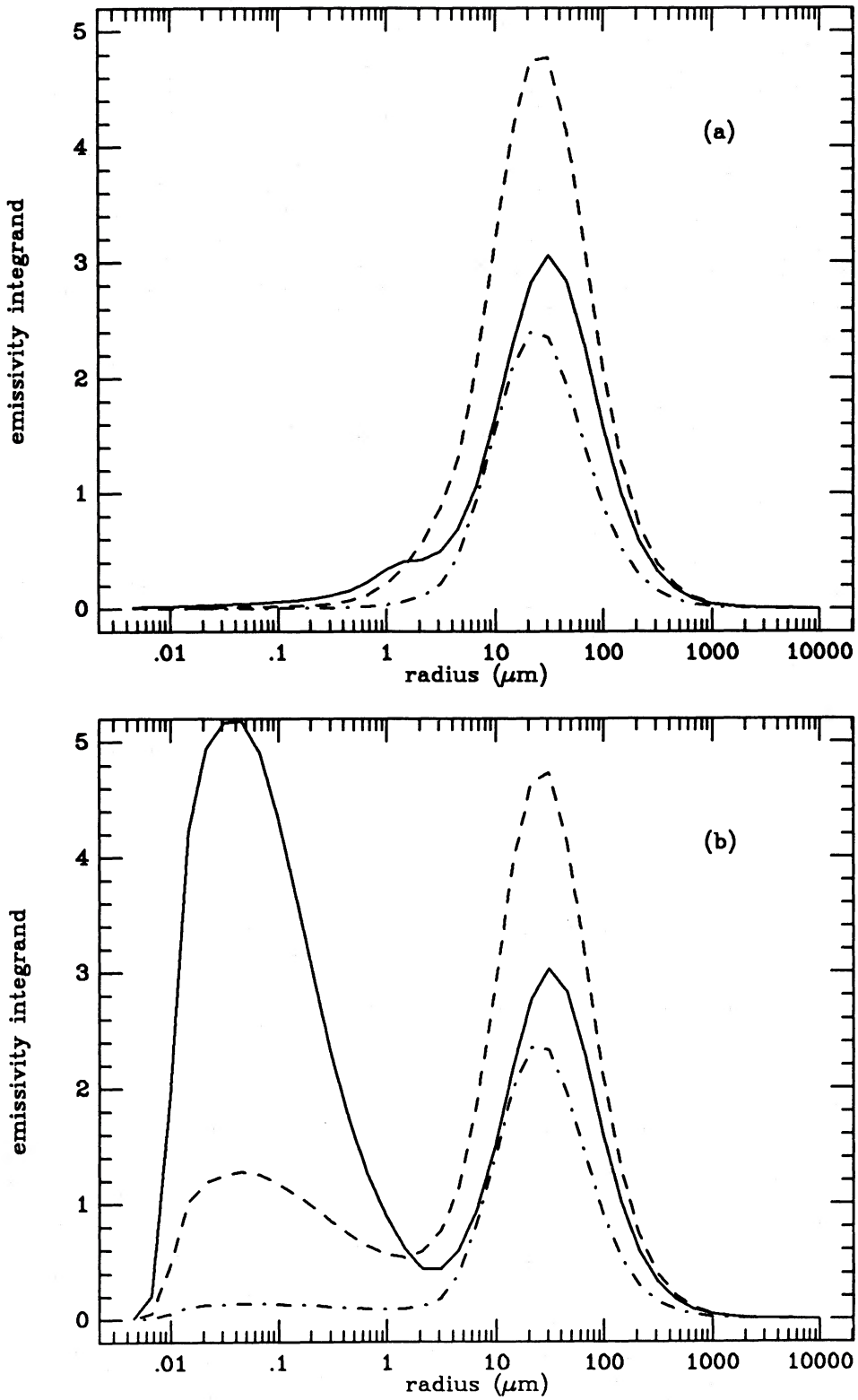

FIG. 4.—Emissivity integrand as a function of particle radius for "constantite" ($m = 1 - i$) spheres illuminated by the solar flux at the Earth's orbit. Curves correspond to the 12 μm (*solid*), 25 μm (*dashed*), and 60 μm (*dash-dot*) emissivity integrands. (*a*) Interplanetary size distribution. (*b*) Lunar size distribution. The "submicron" population produces the peak at particle radius ~0.03 μm, and the "classical" population produces the peak at ~20 μm.

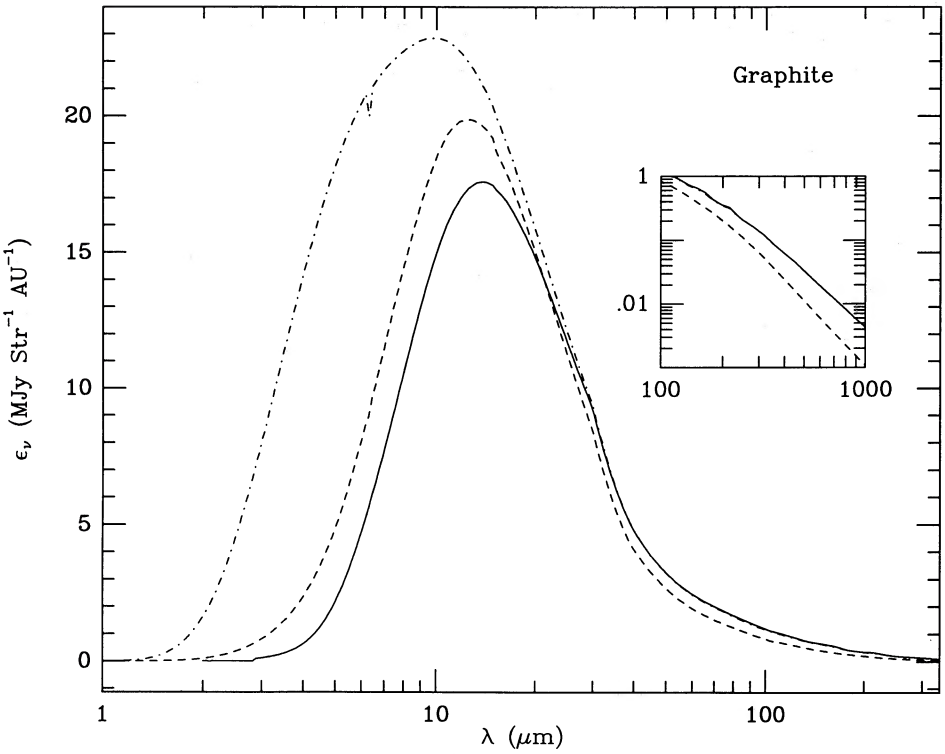

FIG. 5*a*

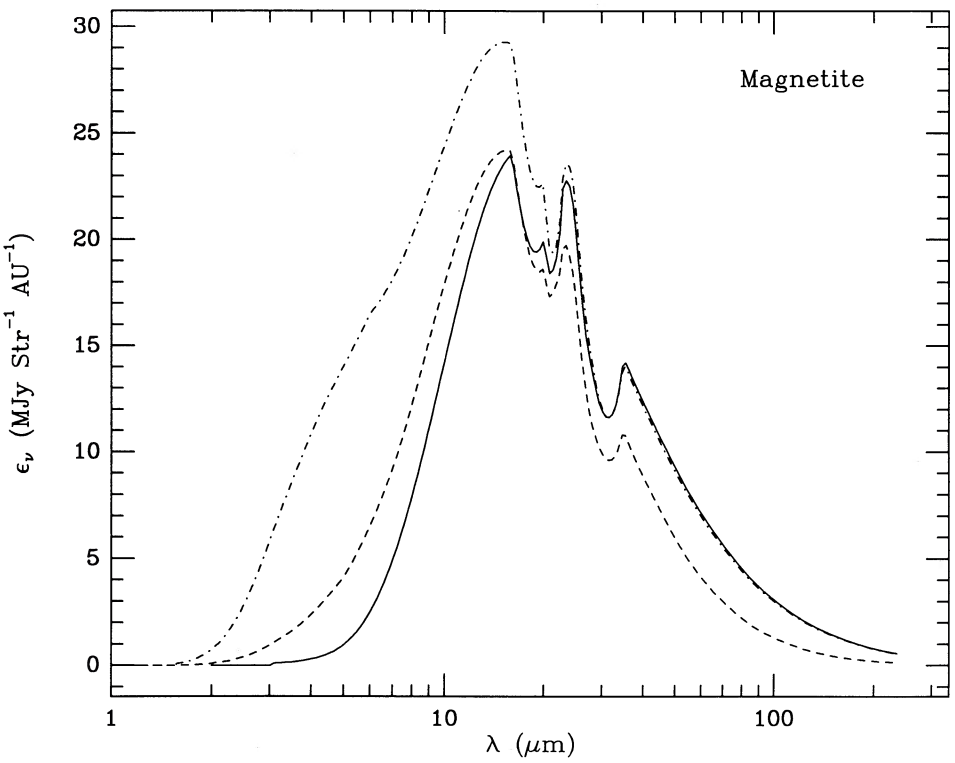

FIG. 5*b*

FIG. 5.—Emission spectra predicted by the models of § II, for (*a*) graphite, (*b*) magnetite, (*c*) "astronomical silicate," (*d*) andesite, and (*e*) obsidian. The curves in each panel correspond to the "interplanetary" size distribution (*solid*), the "lunar" size distribution (*dotted*), and the "Halley" size distribution (*dashed*). The emissivity units are MJy sr^{-1} AU^{-1}; in the cgs system, one unit corresponds to 6.68×10^{-31} ergs cm^{-3} s^{-1} Hz^{-1} sr^{-1}. The insets in panels *a* and *c* show the spectrum from 100 to 1000 μm on a logarithmic scale.

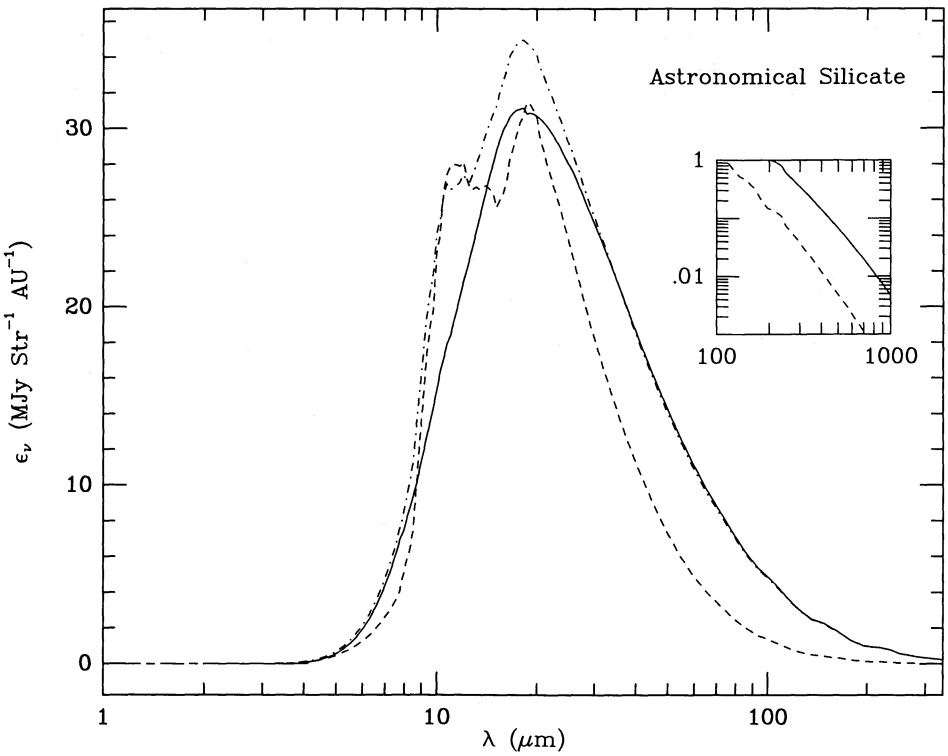

FIG. 5c

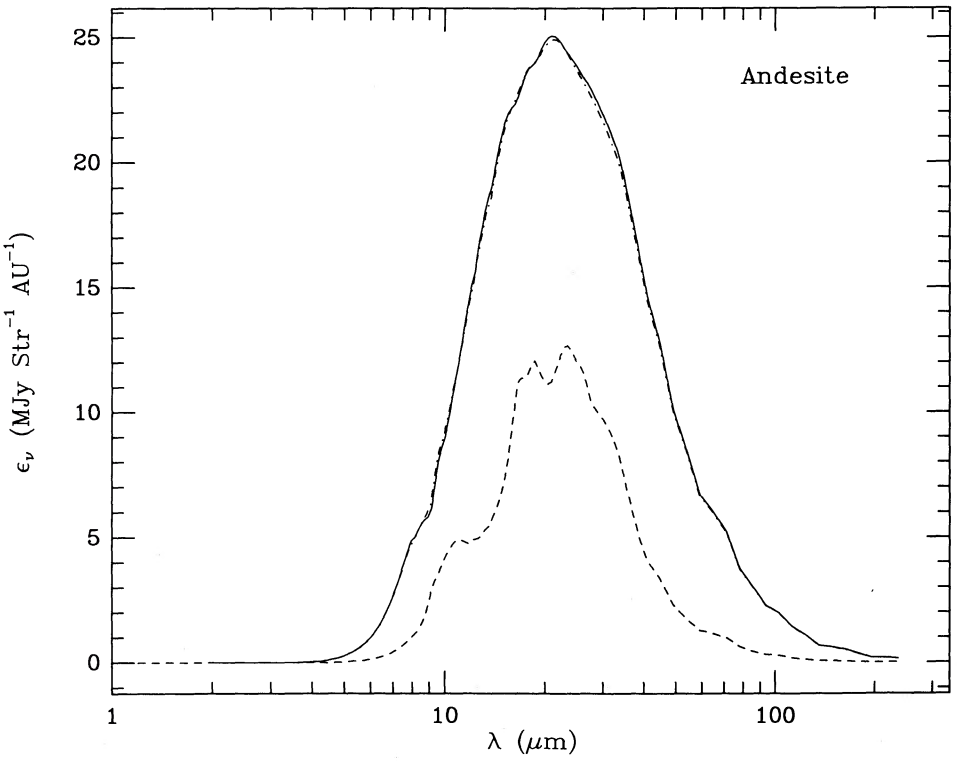

FIG. 5d

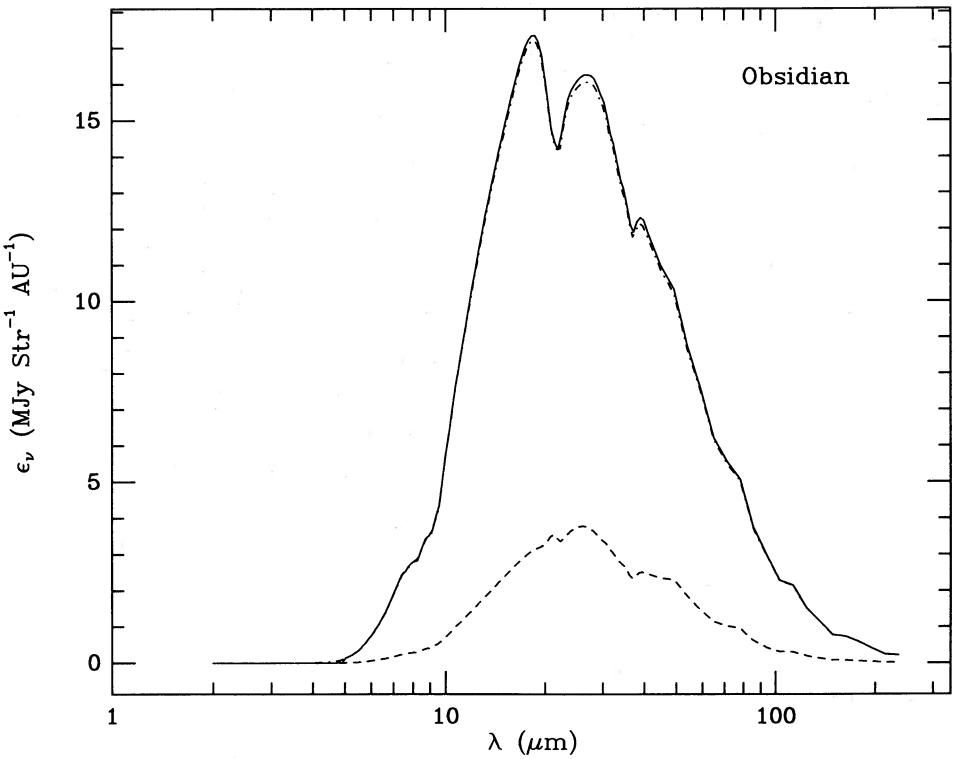

FIG. 5e

The spectra for obsidian (Fig. 5e), and andesite with the Halley size distribution, are the most peculiar. Two features appear in *apparent absorption* at 22 and 35 μm for obsidian. (From an optically thin cloud, there can be no true absorption features.) Thermal emission at 10 μm is negligible for andesite and obsidian grains, so the 10 μm feature is unobservable. The 22 μm line is due to Si-O-Si stretch vibrations; the cause of the 35 μm feature is unknown to this author, but it is present in the reflectance data of Pollack, Toon, and Khare (1973). The lines are carried by large grains. Obsidian grains larger than 10 μm have slight dips in absorption efficiency at the location of the 22 and 35 μm lines. The equivalent width of the 22 μm line is ~0.08 μm, which may be detectable in the near future. (The 35 μm line is weaker, with equivalent width ~0.01 μm.)

III. OBSERVATION OF THE LOCAL VOLUME EMISSIVITY

The infrared surface brightness of the zodiacal emission is given by the brightness integral,

$$I_\nu = \int_{\rm LOS} \mathscr{E}_\nu(s) ds \,, \tag{4}$$

where the path of integration begins at the observer and continues along the line of sight until the volume emissivity $\mathscr{E}_\nu(s)$ becomes negligible. Inversion of the brightness integral is possible only in special cases, for which a particular series of observations is required. We present here the results of two simple methods, both of which collapse the brightness integral into the product of a short (or infinitesimal) path length and the local volume emissivity.

a) Brightness in the Ecliptic Plane

The classic inversion technique for determining the volume scattering emissivity from the in-ecliptic brightness of the ZL was derived by Dumont (1972), and was applied to preliminary *IRAS* data by Levasseur-Regourd and Dumont (1986). The most elementary application of the inversion technique is the determination of the local volume emissivity by isolating the contribution to the brightness integral of an infinitesimal secant of the Earth's orbit. The geometry of the method is shown in Figure 6. The difference between the ZE brightness at points *A* and *B* is due to the dust along the short path *AB*. Assuming azimuthal symmetry, the points *A* and *B* need not be located as shown in the diagram, as long as the solar elongation angles of the line of sight satisfy $\epsilon_A + \epsilon_B = 180°$. The local emissivity is obtained in the limit when the path *AB* becomes infinitesimal. In terms of the angle $\theta = 90° - \epsilon_B$,

$$\left.\frac{dI_\nu}{d\theta}\right|_{\theta=0} = \lim_{\theta\to 0} \frac{I_\nu(B) - I_\nu(A)}{2\theta} = \mathscr{E}_\nu(1\ \mathrm{AU}) d_0 \,, \tag{5}$$

where d_0 is the distance 1 AU. (For arbitrary *AB*, information about the zodiacal emissivity at smaller heliocentric distances is found; this fact is exploited in Reach 1988, hereafter Paper II.)

In order to determine the local volume emissivity using equation (5), the variation of the ZE brightness in the ecliptic plane must be observed for a range of solar elongation angles (ϵ) around 90°. *IRAS* observations covered the range of ϵ from 60° to 120° during HCON 3 (1983 August 26 to 1983 November 22), and the Zodiacal Observation History File provides

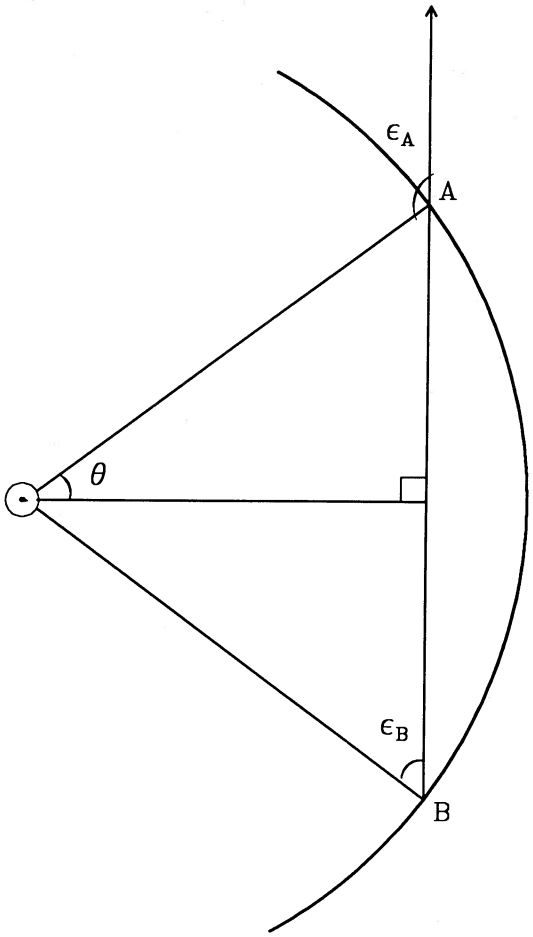

FIG. 6.—Geometry of the inversion method. The difference between the brightness observed at points *A* and *B* of the Earth's orbit, along the shown line of sight, is due to the dust along the chord *AB*.

the data required to determine the ZE brightness as a function of ϵ with $\sim 0.^{\circ}5$ angular resolution (*IRAS Explanatory Supplement* 1985). We have used this data set to construct two-dimensional maps of the brightness in the coordinate system of solar elongation and ecliptic latitude (Reach and Heiles 1988). Slices through these maps in the ecliptic plane were fitted with orthogonal polynomials, and the derivatives required for equation (5) were calculated from the coefficients.

Lines of sight with Galactic latitude $|b| < 10^{\circ}$ were excluded from the fits. Additional terms were included in the fit in order to remove systematic uncertainties, as discussed in Paper II. Crucial to the 60 and 100 μm fits was a term proportional to Galactic H I column density, which was obtained from the Hat Creek 21 cm survey of Heiles and Habing (1974). Significant at 12 and 25 μm was a nonlinear term modeling the effect of the eccentricity of the Earth's orbit (Paper II). The resulting values of the local emissivity are listed in Table 1, together with the statistical uncertainties obtained from the coefficients of the least-squares fits.

b) *Annual Polar Brightness Variation*

The brightness of the zodiacal light observed toward the ecliptic poles varies with a period of 1 yr, as has been known for some time (e.g., Dumont and Levasseur-Regourd 1978). This variation is interpreted as the effect of the changing position of the Earth with respect to the hypothetical symmetry plane of the zodiacal cloud. We assume that the dust distribution is azimuthally symmetric about an axis that passes through the Sun, and that it is reflection-symmetric about the symmetry plane, which intersects the ecliptic in a line of nodes passing through the Sun. (The accuracy of these assumptions is high, as we know from the regularity of the zodiacal light over full years of observation, both by *IRAS* and ground-based optical telescopes and from the ability of symmetric models to reproduce the infrared brightness profiles [e.g., Hauser 1988].)

The geometry of the symmetry plane is shown in Figure 7. As the Earth completes an orbit about the Sun, the distance h from the Earth to the symmetry plane varies sinusoidally with orbital phase ϕ (measure relative to the line of nodes). By symmetry, the polar brightness difference is equal to twice the integral of the emissivity over the path beginning at the observer and ending at the symmetry plane. (A small error is introduced by using the ecliptic pole instead of the pole defined by the line perpendicular to the symmetry plane.) Since the inclination of the symmetry plane with respect to the ecliptic is small ($i \simeq 1.^{\circ}8$; see below) the path length is short ($0 \leq h \lesssim 0.03$ AU). Thus the volume emissivity may be expanded in a Taylor series about the symmetry plane, and the polar brightness difference is

$$I_\nu(\mathrm{NEP}) - I_\nu(\mathrm{SEP}) \simeq 2\mathscr{E}_\nu(1\ \mathrm{AU}) d_0 \sin i \sin \phi \ . \qquad (6)$$

In this equation I_ν(NEP) and I_ν(SEP) are the surface brightnesses measured toward the north and south ecliptic poles, respectively, and d_0 is the distance 1 AU.

Although the *IRAS* observations reveal a nearly sinusoidal polar brightness variation as expected from equation (6), there are some systematic errors. The primary cause for deviation from a sinusoidal variation is the eccentricity of the Earth's orbit (Reach and Heiles 1988). This effect causes an annual modulation of the polar brightness that is evident in the annual variation of the polar brightness *sum*. The polar brightness *difference* is only slightly affected. The expected amplitudes of the modulation of the zodiacal emissivity at the Earth's orbit, due to the radial gradients in grain temperature and density, are 6%, 4%, 4%, and 3% at 12, 25, 60, and 100 μm, respectively, using density proportional to $r^{-1.3}$ (Lienert *et al.* 1981) and temperature proportional to $r^{-0.5}$. Since the phase of this modulation is determined by the perihelion of the Earth's orbit, a single nonlinear term was needed to model the eccentricity effect in the least-squares fits (cf. Paper II). The polar brightness difference fits were found to be quite insensitive to the eccentricity effect.

Another possible cause for deviation from a sinusoidal variation is higher order terms in the expansion of the emissivity. Since the dust distribution is even about the symmetry

TABLE 1

VOLUME EMISSIVITY FROM SECANT METHOD

Parameter	12 μm	25 μm	60 μm	100 μm
$\mathscr{E}_\nu(1\ \mathrm{AU})$[a]	3.31	4.94	1.45	0.66
σ[b]	0.01	0.01	0.01	0.02

[a] Local volume emissivity, derived using eq. (5), in units of 10^{-29} ergs cm^{-3} s^{-1} Hz^{-1} sr^{-1}.

[b] Statistical uncertainty in emissivity values. Same units.

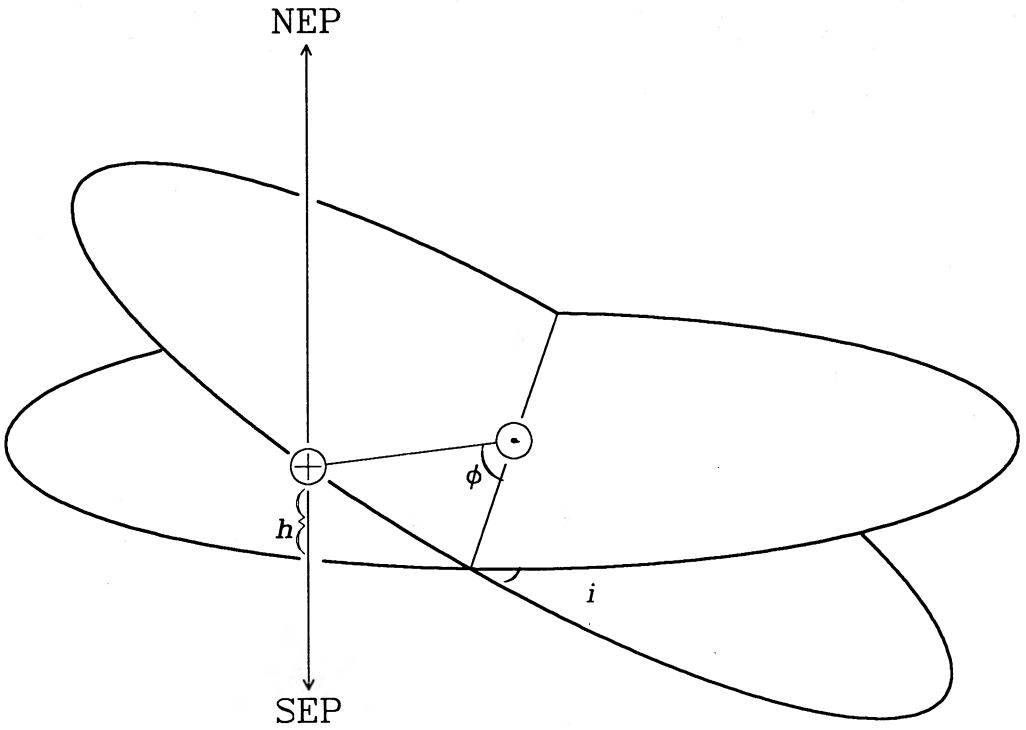

FIG. 7.—The orbit of the Earth shown together with the assumed zodiacal symmetry plane. The inclination i of the symmetry plane is greatly exaggerated for clarity. The difference between the brightness of the NEP and the SEP is due to the dust along the path of length h.

plane, the first derivative of the emissivity must vanish there; therefore, the next important term in the expansion of the emissivity is of second order in h. Using results from modeling the zodiacal light (Giese, Kneissel, and Rittich 1986), the dust density varies by less than 6% over the short path of integration. The grain temperature remains constant to within 0.1% for all grain constituents. Thus the error caused by the exclusion of higher order terms is expected to be very small.

The polar brightness difference measured by *IRAS* over its observing lifetime (1983 February 9 through 1983 November 22) is shown for all four *IRAS* bands in Figure 8. The *IRAS* data were obtained from the Zodiacal Observation History File (version 2, summer 1986; see *IRAS Explanatory Supplement* 1985), which contains a time-ordered list of boxcar-smoothed observations with an effective angular resolution of 0°.5. Observations within 2° of the poles were used, and the polar brightness differences were calculated using data from individual half-orbits, for which the calibration is identical. Observations centered within 0°.6 of the bright planetary nebula NGC 6543 (near the NEP) were excluded to improve the fits. A region round the Large Magellanic Cloud (near the SEP) was also excluded.

We performed a linear least-squares fit to the polar brightness data using a function of the form

$$I_\nu(\mathrm{NEP}) - I_\nu(\mathrm{SEP}) = A_\nu \cos(\lambda_\odot - \Omega) + B_\nu , \qquad (7)$$

where $\lambda_\odot$ is the ecliptic longitude of the Sun (measured relative to the first point in Aries). The amplitudes, A_ν, and their uncertainties are given in Table 2 for the four *IRAS* bands centered at 12, 25, 60, and 100 μm. The values of B_ν and Ω are also shown for each fit. The spectrum and magnitude of the offset, B_ν, are consistent with the difference between the Galactic emission at the NEP and the SEP, which are located at Galactic coordinates (l, b) of (95°, +30°) and (275°, −30°), respectively. The values of Ω from the 12 and 25 μm fits are consistent with each other, while the 60 and 100 μm fits both have somewhat smaller Ω.

Using equation (6) and the volume emissivity obtained by the inversion method of § III*b*, we may solve for the inclination of the symmetry plane from the fit for each *IRAS* wavelength band; the results are shown in Table 2. The agreement among these independently determined values is very good, and we may derive a weighted mean value of $i = 1°.71 \pm 0°.02$. This inclination is consistent with previous determinations based on infrared measurements (cf. Hauser 1988) and optical measurements (cf. Dumont and Levasseur-Regourd 1978). Taken together with the ascending node at longitude $\Omega = 77°.1 \pm 0°.4$, our results imply that the symmetry surface crosses the Earth's orbit in a plane intermediate between the orbital planes of Venus and Mars, as noted by Hauser (1988).

The agreement between the inclinations derived from the polar brightness variations at different wavelengths supports our determination of the spectrum of local dust. Further, the agreement of the magnitude of the inclination of the symmetry plane with previous studies supports the magnitude of the emissivity derived by the inversion method.

IV. DISCUSSION

a) Comparison of Predictions and Observations

i) *Color Correction*

The spectral resolution of diffuse far-infrared background observations is at present very low. It is thus necessary to degrade the predicted spectra of § II to compare them with the observations in § III. In order to convert a predicted spectrum $\mathscr{E}_\nu$ into an "*IRAS*-quoted" equivalent value $\bar{\mathscr{E}}_{\nu_i}$, one must integrate over the instrumental spectral response $R_\nu^{(i)}$ for each band i (*IRAS Explanatory Supplement* 1985, Table II.C.5) and divide

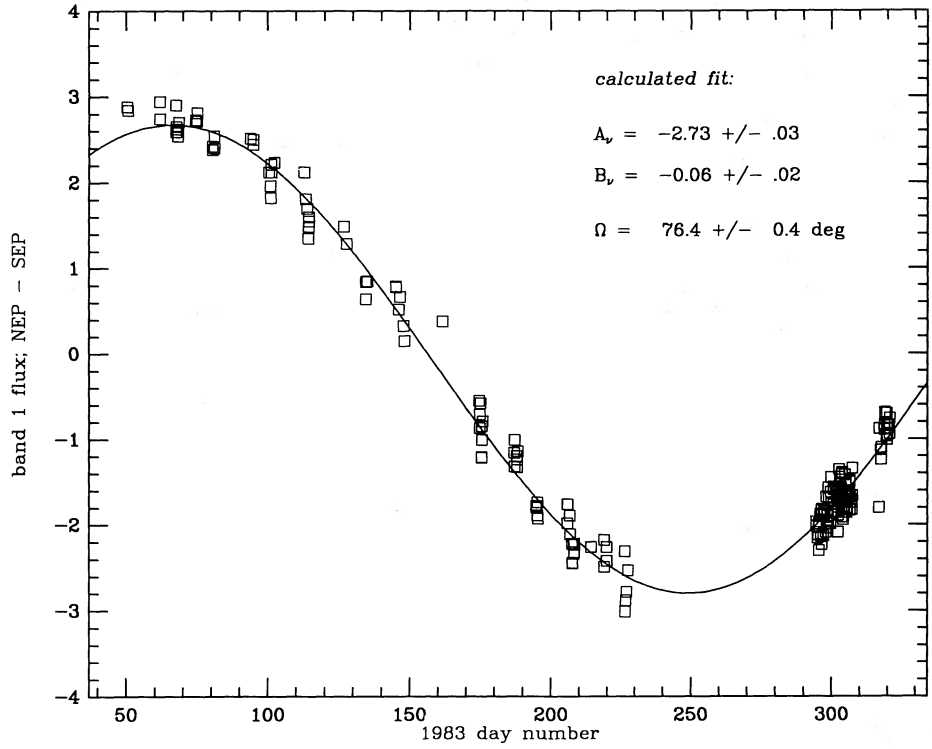

FIG. 8*a*

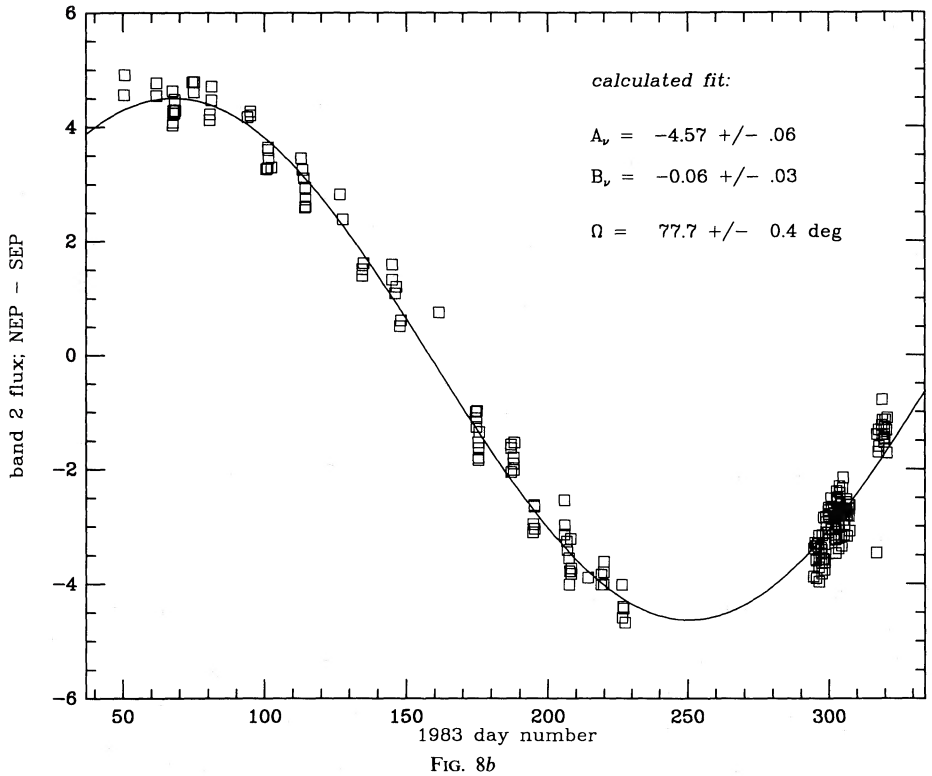

FIG. 8*b*

FIG. 8.—Polar brightness difference as a function of time, during the observing lifetime of *IRAS*, at (*a*) 12 μm, (*b*) 25 μm, (*c*) 60 μm, and (*d*) 100 μm. Points are the actual *IRAS* data, and the curves are the least-squares cosine fits. The amplitude, phase, and offset of the fit are shown in the upper right-hand corner of each panel.

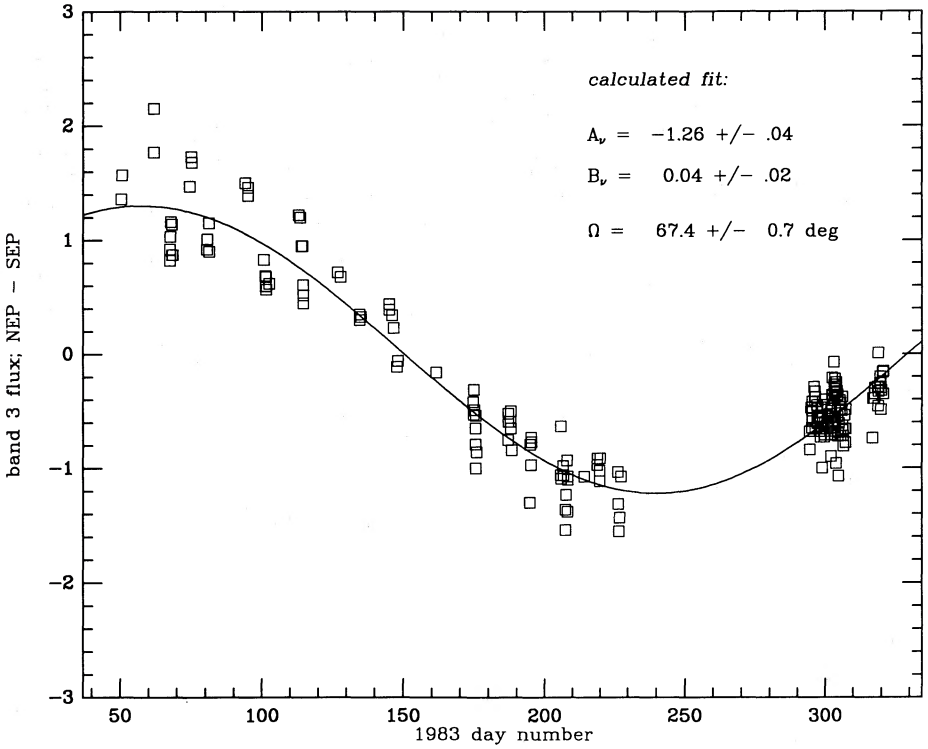

FIG. 8*c*

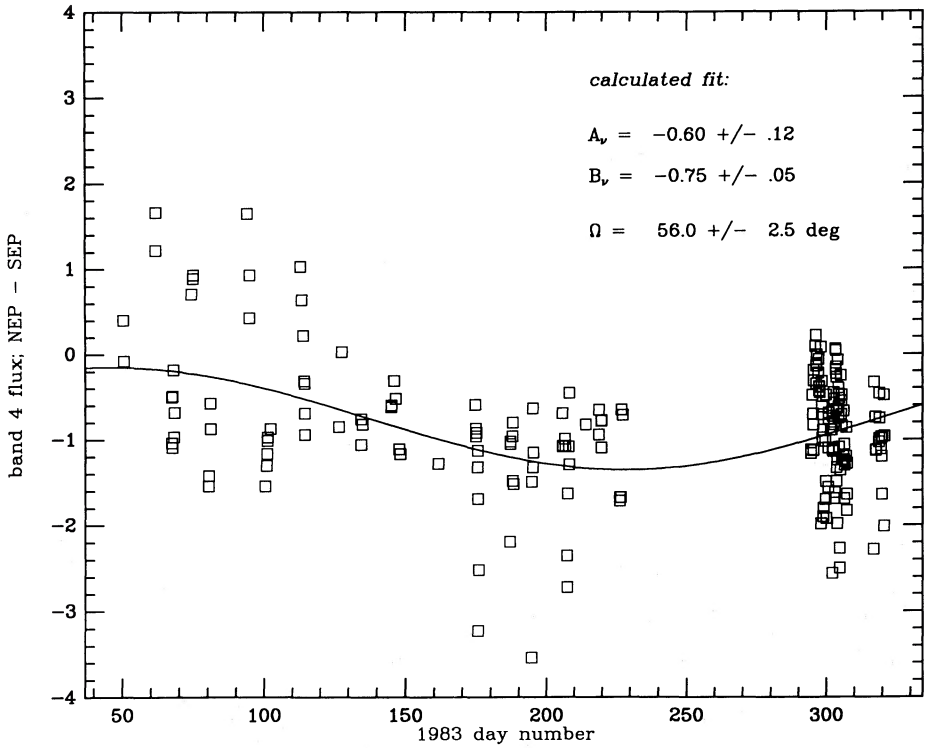

FIG. 8*d*

TABLE 2

ANNUAL POLAR BRIGHTNESS VARIATION

Parameter	12 μm	25 μm	60 μm	100 μm
A^a	2.73 ± 0.03	4.57 ± 0.06	1.26 ± 0.04	0.60 ± 0.12
B^a	−0.06 ± 0.02	−0.06 ± 0.03	0.04 ± 0.02	−0.75 ± 0.05
Ω^b	76.4 ± 0.4	77.7 ± 0.4	67.4 ± 0.7	56.0 ± 2.5
i^c	1.71 ± 0.02	1.77 ± 0.03	1.51 ± 0.05	1.77 ± 0.01

[a] Parameters defined in eq. (7), with 1 σ statistical uncertainties, in units of 10^{-17} ergs cm^{-2} Hz^{-1} sr^{-1}.

[b] Longitude of ascending node of symmetry plane, in degrees.

[c] Inclination of symmetry plane, derived from A-values (see text).

out the same integral over the assumed spectrum (proportional to ν^{-1}; *IRAS Explanatory Supplement* 1985, § VI.C.3):

$$\tilde{\mathscr{E}}_{\nu_i} = \int \mathscr{E}_\nu R_\nu^{(i)} d\nu \Big/ \int (\nu/\nu_i)^{-1} R_\nu^{(i)} d\nu \,. \quad (8)$$

The results are shown in Table 3, for each grain constituent and the three size distribution models, for the *IRAS* 25 μm band, together with the ratios of the 12, 60, and 100 μm band results to those in the 25 μm band.

ii) *Overall ZE Brightness*

One result is immediately obvious from comparing the values in Table 3 with those in Table 1: The predicted emissivities are smaller than the observed emissivity by a factor of ~2. This difference cannot be easily explained, but it could be of crucial importance for understanding the physical properties of interplanetary dust. Two instrumental explanations exist: *IRAS* brightnesses were overestimated, or the particle fluxes were underestimated. Since the *IRAS* data used in this paper are differences between observations with identical calibration, the *IRAS* error must be in the *gain*. The *absolute* calibration (zero level) cancels out. The *IRAS* calibration is tied directly to point-source observations (*IRAS Explanatory Supplement* 1985, § VI.C.4), which have been extensively checked with prior observations of stars and asteroids.

It must be noted that the brightness of the ZE observed by the rocket-borne detectors of Murdock and Price (1985) is a factor of ~2 lower than that observed by *IRAS*. Hong and Um (1987) used the rocket data to invert the ZE brightness integral, and they derived 10.9 and 20.9 μm emissivities of 1.6×10^{-29} and 1.9×10^{-29} ergs cm^{-3} s^{-1} Hz^{-1} sr^{-1}, respectively. These values are only half as large as those obtained from the *IRAS* data (§ III), but the 10.9/20.9 μm ratio is consistent with that obtained from the *IRAS* data. Thus the predictions of § II are consistent with Murdock and Price's observations.

The second instrumental explanation for the discrepancy between the predicted and *IRAS*-observed ZE brightness is that particle-flux measurements described in § II*c* are systematically low. Such an error is quite possible for these observations, which span some 20 orders of magnitude of particle flux. However, the agreement between the two completely independent methods of determining particle flux (from the lunar microcrater distribution and satellite measurements) for large particles lends support to the calibration of the particle-flux measurements.

There are also theoretical reasons why the ZE predictions in this paper could be too low. We have assumed homogeneous, spherical grains, whereas interplanetary dust collected in the stratosphere, deep-sea sediments, and arctic ices ranges in morphology from smooth and spherical to rough, irregular, and highly porous (Brownlee 1985). The accuracy of Mie theory for such particles is questionable. Since particle detectors of the "beer can" type are sensitive to the area of the holes caused by particles penetrating a foil, the distribution of particles as a function of geometric cross section is observed. Thus an explanation based on particle morphology must explain the factor of 2 difference by enhanced absorption efficiency of porous particles relative to that of solid particles with the same geometric cross section. The fractal grain model of Wright (1987) reveals that porous grains are in fact better absorbers than are spheres, but this theory applies only in the small-particle limit and cannot yet be applied to the ZE.

iii) *Spectrum*

Since the overall brightness of the ZE differs among observations by a factor of 2, we are forced to constrain the constituent of interplanetary dust using the spectral shape alone. We assume here that the discrepancy in the overall brightness of the ZE is due to calibration errors. Let us define C_λ to be the ratio of the volume emissivity at wavelength λ to that at 25 μm. The predicted ratios are shown in the last three columns of Table 3 for the models of § II. From Table 1 the observed values and (statistical) uncertainties of these ratios are $C_{12} = 0.67 \pm 0.01$, $C_{60} = 0.32 \pm 0.01$, and $C_{100} = 0.13 \pm 0.01$.

1. *Short-wavelength color.*—The short-wavelength color (C_{12}) best constrains the grain temperature and the contribution of submicron grains, because it samples the Wien portion of the spectrum. The graphite and magnetite spectra, for all three size distributions, are inconsistent with C_{12} to a high level of significance. Small particles of these materials become very hot, and they produce substantial 12 μm emission. Small silicate particles, on the other hand, are cool. C_{12} is somewhat too low for obsidian and andesite, for all three size distributions. The "Halley" size distribution produces C_{12} values which are too high for graphite, magnetite, and astronomical

TABLE 3

PREDICTED EMISSIVITY IN *IRAS* BANDS

Constituent	ϵ_ν(25 μm)[a]	12/25	60/25	100/25
A. "Interplanetary" Size Distribution				
Graphite	0.98	1.19	0.21	0.09
Magnetite	1.42	0.85	0.41	0.15
Astronomical silicate	2.15	0.60	0.41	0.16
Andesite	1.78	0.48	0.35	0.08
Obsidian	1.15	0.50	0.51	0.17
"Dirty" andesite[c]	2.29	0.57	0.30	0.08
B. "Lunar" Size Distribution				
Graphite	1.04	1.52	0.20	0.08
Magnetite	1.54	1.23	0.37	0.14
Astronomical silicate	2.30	0.73	0.38	0.15
Andesite	1.77	0.48	0.34	0.08
Obsidian	1.18	0.49	0.50	0.17
C. "Halley" Size Distribution				
Graphite	0.96	1.41	0.18	0.06
Magnetite	1.26	1.10	0.29	0.08
Astronomical silicate	1.92	0.81	0.23	0.05
Andesite	0.85	0.35	0.18	0.27
Obsidian	0.25	0.31	0.48	0.12

[a] Emissivity averaged over *IRAS* 25 μm band, in units of 10^{-29} ergs cm^{-3} s^{-1} Hz^{-1} sr^{-1}.

[b] Arbitrarily normalized to the interplanetary size distribution at particle radius $a = 10$ μm.

[c] Andesite with 3% (by volume) graphite impurities.

silicate, and too low for andesite and obsidian. The *only* model which is within the observational uncertainty is astronomical silicate with the "interplanetary" size distribution.

2. *Long-wavelength color.*—The ZE spectrum at wavelengths longer than the peak (~ 20 μm) is most sensitive to the long-wavelength optical properties of the constituent material and the slope of the size distribution for large, "classical" grains. Obsidian is clearly inconsistent (>6 σ) with the observed C_{60} for all three size distributions. Several other models, including "astronomical silicate," are marginally inconsistent with C_{60} (at the 1–3 σ level). The 100 μm color is not as well contrained by the *IRAS* observations. Graphite models have values of C_{100} which are somewhat high, and andesite models have somewhat low values. Thus, no model provides a good fit at all *IRAS* wavelengths.

An upper limit at 225 μm may be added using the observations of Salama *et al.* (1987). Since these observations are not absolutely calibrated, we scale their 225 μm brightness limit to their 100 μm brightness and multiply by the *IRAS* 100 μm emissivity; the result is $C_{225} < 0.03$. Optical data at 225 μm were available only for graphite and astronomical silicate, both of which produced 225 μm colors ($C_{225} \simeq 0.025$ for graphite, 0.030 for astronomical silicate) just consistent with the upper limit.

b) *Improved Models for Interplanetary Dust*

Since homogeneous grains of a variety of constituent materials cannot explain the overall brightness of the ZE, we have investigated some more complicated models. The improved models must produce more emission and remain consistent with the observed spectrum (especially the 12/25 μm color). One obvious class of models is linear combinations of separate populations of homogeneous grains. Using the results of § II, it is not possible to increase the brightness of the ZE significantly with a linear combination. The spectrum for pure silicates (andesite and obsidian) can be improved by adding a small population of carbonaceous grains. We find that the number density of graphite grains must be less than 5% of that of silicate grains in order to remain consistent with the observed color temperature. This constrains the fraction of carbonaceous grains in the interplanetary medium to be smaller than that of "CHON" particles (35%; Langevin *et al.* 1987) observed in the coma of comet P/Halley.

In this section we discuss inhomogeneous, spherical grains consisting of silicates and graphitic "dirt." Silicates are necessary to explain the 10 μm features observed in the spectra of interplanetary dust collected in the stratosphere (Sandford and Walker 1985) and in the spectra of comets (Hanner 1980). We use andesite (Pollack, Toon, and Khare 1973) as our silicate in this section. Dirt is included to increase the opacity of the grains to sunlight, thereby increasing the grain temperature.

The effect of dirt on the optical properties of a grain depends on its distribution within the particle. We considered three models: (1) a graphitic shell around a silicate core, (2) a graphitic core within a silicate shell, and (3) a well-mixed solid. For each model, the amount of dirt is specified by its volume filling factor within the grain. The absorption efficiency for coated spheres was calculated using the computational method of Toon and Ackerman (1981), who performed similar calculations in order to determine the effect of graphitic soot on absorption of visible light by particles in the terrestrial atmosphere. The well-mixed case (case 3) was calculated using the Maxwell-Garnett law (cf. Chýlek and Srivastava 1983), which defines a dielectric constant for the effectively homogeneous medium; standard Mie theory was then used to calculate the absorption efficiency.

The temperature of dirty grains was consistently greater than of clean grains, as expected. The results for a volume filling factor of 3% graphite are illustrative. Large ($a > 20$ μm) graphitic-core and well-mixed (cases 1 and 3) approach the temperature of clean silicate grains. Large graphite-shell grains (case 2, $a > 5$ μm), on the other hand, approach the temperature of pure graphite grains; the shells are optically thick both to sunlight and emitted infrared. The dependence of temperature on particle size is complicated for smaller grains. In the small-particle limit the temperatures are 500 K (case 1), 200 K (case 2), and 320 K (case 3).

The emission spectra of the three types of dirty grains (with 3% graphite) are shown together with that of clean andesite in Figure 9. (The interplanetary size distribution (§ IIc) was used for these spectra.) It is evident that graphitic-shell (case 1) particles are too hot and produce a spectrum which is inconsistent with the observed 12 μm color. The graphitic-core (case 2) spectrum is nearly identical with that of clean particles. Only the well-mixed (case 3) spectrum is brighter than for clean grains; the *IRAS* 25 μm band-averaged emissivity is 29% larger. Further, the color ratios of the case 3 spectrum fit the *IRAS*-observed color ratios better than any of the homogeneous-particle models; we obtain we obtain $C_{12} = 0.58$, $C_{60} = 0.30$, and $C_{100} = 0.07$. However, the 25 μm brightness is still a factor of 2 lower than observed by *IRAS*. Larger volume fractions of graphite increase the 25 μm brightness, but at the expense of increasing the color temperature of the spectrum. The largest volume filling factor which is consistent with the 3 σ observational range of C_{12} is 5%.

Note that the case 3 emission spectrum is very similar to that of the astronomical silicate (Fig. 5). The dielectric function predicted by the Maxwell-Garnett law for andesite with 3% is nearly identical with the dielectric function of astronomical silicate. The only significant differences are a lower value of the absorptivity longward of 30 μm and a more pronounced 10 μm emission band. Thus astronomical silicate grains, which have been used to model the interstellar extinction curve and infrared emission features, may be interpreted as silicate grains with some 3% graphitic impurity. Since both larger and smaller levels of impurity are inconsistent with the ZE spectrum, this is evidence that interplanetary silicate grains are similar to interstellar silicate grains.

The ZE spectra of dirty silicates reveal no emission features. This result is not surprising, since large particles, which do not carry the emission features, dominate the emission. Reflection spectroscopy of intimate mixtures of different particulate materials (charcoal volcanic soil, and clay) with ice reveal that the near-infrared reflectance and ice absorption-band depths depend sensitively on the abundance of the particulates (Clark and Lucey 1984). By analogy, the 10 and 20 μm silicate features produced by a silicate-graphite mixture may be different from the homogeneous materials. Our simple approximation neglects particulate scattering within the grain and therefore will not predict accurate line profiles.

c) *Comparison with Cometary Spectra*

Comets are bright enough to be observed with high spectral resolution, and they may be observed over a range of heliocentric distances. Since the spatial extent of the cometary coma is much smaller than 1 AU, all grains of a given size are at the

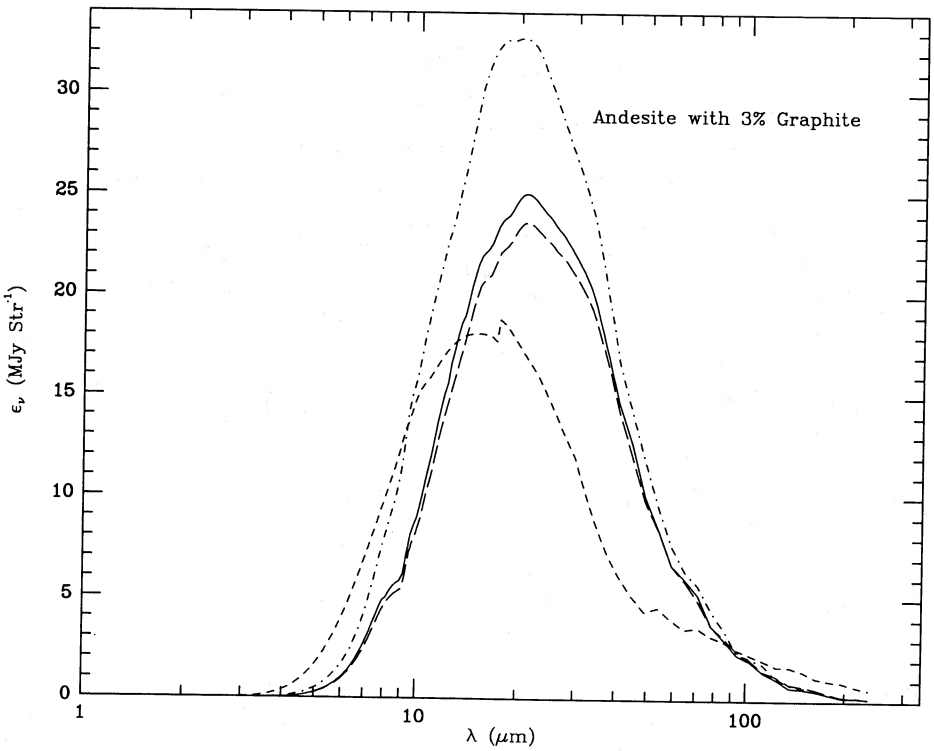

FIG. 9.—Emission spectra predicted for andesite with 3% graphite impurity, together with the pure andesite emission spectrum (*solid line*). Case 1 (graphite coating on andesite sphere) is shown by the short-dashed line, case 2 (andesite coating on graphite sphere) by the long-dashed line, and case 3 (well-mixed) by the dash-dot line.

same temperature. Thus the models of § II apply equally well to comets, as long as the heliocentric distance is calculated at the epoch of observation of the comet. We have used our model to fit the spectrum between 3 and 20 μm of comet P/Halley, at a heliocentric distance of 0.89 AU (Hanner *et al.* 1987; see their Fig. 6). Graphite is clearly ruled out, for the same reason that it is inconsistent with the ZE (excess short-wavelength emission). Further, the 10 μm feature is seen in emission, demonstrating the presence of small silicate grains. Using the Halley size distribution, the 10 μm emission feature is predicted for all silicate minerals. The silicate spectra are too steep in the near-infrared. This situation is alleviated if the grain temperature is increased by opaque impurities. A model with andesite and 3% graphite impurity provides a better fit to the data; a lower impurity level is inconsistent with the data.

Observations of comets in the visible also have some bearing on the dust constituent. Mukai, Mukai, and Kikuchi (1987) have shown that the phase-angle and wavelength dependence of the optical polarization is most consistent with a complex index of refraction $m \simeq 1.4 - 0.03i$ at visible wavelengths. Lamy, Grün, and Perrin (1987) showed that astronomical silicate and graphite both fit their data on the phase-angle dependence of the polarization. (Mukai *et al.* did not cover enough of the complex plane of m-values to find that graphite is consistent with the data.) The index of refraction at visible wavelengths determines the grain temperature. Andesite with 3% graphite impurity and astronomical silicate have indices of refraction which agree with the values obtained from optical polarization.

V. CONCLUSIONS

We have calculated the emission spectra of interplanetary dust for five different constituent materials and three size distributions, and compared them with the spectrum of the zodiacal emission as observed by *IRAS*. The two most important constraints on interplanetary dust models are the overall brightness of the ZE and the color temperature of the emission spectrum. No single type of homogeneous grain is consistent with both of these constraints. Homogeneous spheres of the hypothetical material "astronomical silicate" (DL) produce a spectrum with the correct color temperature. Andesite, with 3% by volume graphite impurity, provides the best fit to the spectral shape. Metallic grains (graphite and magnetite) produce spectra which are much too "hot," and pure dielectric grains (andesite and obsidian) produce spectra which are somewhat "cold." These conclusions are in accord with those of Frazier, Boucher, and Mueller (1987), who further showed that graphite and magnetite grains produce optical polarization with a distribution inconsistent with ZL observations.

None of the predicted spectra are consistent with the overall ZE brightness reported by *IRAS*. Adding more impurities to the silicates increases the predicted color temperature beyond the allowable range. Linear combinations of separate populations of carbonaceous and silicate grains do not increase the brightness of the ZE. Indeed, the carbonaceous component must have a number density at most 20 times smaller than that of the silicate component, indicating that the "CHON" particles found in the coma of P/Halley do not comprise a substantial fraction of interplanetary dust.

The uncertainty in the ZE brightness will be resolved by future space missions. Murdock and Price (1985) report a ZE brightness which is fully consistent with our predictions, differing from *IRAS* by a factor of 2. The Cosmic Background Explorer (COBE) satellite will provide well-calibrated spectra of the infrared background radiation. The Diffuse Infrared Background Experiment (DIRBE) on COBE has four detec-

tors which are similar in wavelength response to the *IRAS* detectors and can thus be directly compared with the low angular resolution (0°.5) *IRAS* data.

The contribution of the ZE to the infrared background from 3 to 1000 μm is predicted for graphite and astronomical silicate (see Fig. 5). Our results may be used to calculate the ZE brightness along a given line of sight by specifying the density distribution in the zodiacal cloud. (The grain temperatures scale as $d^{-0.5}$ for most constituents and grain sizes; see Paper II.) COBE observations will cover from 1 to 300 μm with DIRBE and from 0.1 to 10 mm with the Far Infrared Astronomical Spectrometer (FIRAS). The short-wavelength DIRBE detectors will constrain the numbers of hot interplanetary dust particles, while the long-wavelength DIRBE and FIRAS detectors will constrain the optical properties of the grain material. Combined with continued collection and measurement of stratospheric and arctic interplanetary dust, future observations of the ZE will continue to provide important information on the composition of interplanetary dust.

This work was supported by a National Aeronautics and Space Administration (SADAP) grant to Dr. Carl Heiles, to whom the author is greatly indebted for many suggestions and criticisms of the present paper.

REFERENCES

Allen, C. W. 1973, *Astrophysical Quantities* (London: Athlone).
Bernatowicz, T., Fraundorf, G., Ming, T., Anders, E., Wopenka, B., Zinner, E., and Fraundorf, P. 1987, *Nature*, **330**, 728.
Bohren, C. F., and Huffman, D. F. 1983, *Absorption and Scattering of Light by Small Particles* (New York: Wiley).
Briotta, D. A. 1976, Ph.D. thesis, Cornell University.
Brownlee, D. E. 1985, *Ann. Rev. Earth Planet. Sci.*, **13**, 147.
Bussoletti, E., Colangeli, L., and Orofino, V. 1987, *Ap. J. (Letters)*, **321**, L87.
Chýlek, P., and Srivastava, V. 1983, *Phys. Rev. B*, **27**, 5098.
Clark, B. C., Mason, L. W., and Kissel, J. 1987, *Astr. Ap.*, **187**, 779.
Clark, R. N., and Lucey, P. G. 1984, *J. Geophys. Res. B*, **89**, 6341.
Colangeli, L., Capozzi, V., Bussoletti, E., and Minafra, A. 1986, *Astr. Ap.*, **168**, 349.
Draine, B. T., and Lee, H. M. 1984, *Ap. J.*, **285**, 89 (DL).
Dumont, R. 1972, *C.R. Acad. Sci., Paris*, **275**, 765.
Dumont, R., and Levasseur-Regourd, A. C. 1978, *Astr. Ap.*, **64**, 9.
Frazier, E. N., Boucher, D. J., and Mueller, G. F. 1987, *Infrared Technology XIII* (*Proc. SPIE*, **819**, 2).
Giese, R. H., Kneissel, B., and Rittich, U. 1986, *Icarus*, **68**, 395.
Giese, R. H., and Lamy, P., eds. 1985, *Properties and Interactions of Interplanetary Dust* (Boston: Reidel).
Grün, E., Zook, H. A., Fechtig, H., and Giese, R. H. 1985, *Icarus*, **62**, 244.
Halliday, I., and McIntosh, B. A., eds. 1980, *IAU Symposium 90, Solid Particles in the Solar System* (Boston: Reidel).
Hanner, M. S. 1980, in *IAU Symposium 90, Solid Particles in the Solar System*, ed. I. Halliday and B. A. McIntosh (Boston: Reidel), p. 223.
Hanner, M. S., Tokunaga, A. T., Golisch, W. F., Griep, D. M., and Kaminski, C. D. 1987, *Astr. Ap.*, **187**, 653.
Hauser, M. G. 1988, in *Proc. Third Internat. IRAS Conf., Comets to Cosmology*, ed. A. Lawrence (Lecture Notes in Physics; Berlin: Springer-Verlag).
Hauser, M. G., *et al.* 1984, *Ap. J. (Letters)*, **278**, L15.
Heiles, C., and Habing, H. J. 1974, *Astr. Ap. Suppl.*, **14**, 1.
Hong, S. S., and Um, I. K. 1987, *Ap. J.*, **320**, 928.
Huffman, D. R. 1977, *Adv. Phys.*, **26**, 129.
Huffman, D. R., and Stapp, J. L. 1973, in *IAU Symposium 52, Interstellar Dust and Related Topics*, ed. J. M. Greenberg and H. C. van de Hulst (Boston: Reidel), p. 297.
IRAS Catalogs and Atlases, Explanatory Supplement. 1985, ed. C. Beichman, G. Neugebauer, H. J. Habing, P. E. Clegg, and T. J. Chester (Washington, DC.: GPO).
Kerker, M. 1969, *The Scattering of Light and Other Electromagnetic Radiation* (New York: Academic).
Lamy, P. L., Grün, E., and Perrin, J. M. 1987, *Astr. Ap.*, **187**, 767.
Lang, K. R. 1980, *Astrophysical Formulae* (New York: Springer-Verlag).
Langevin, Y., Kissel, J., Bertaux, J.-L., and Chassefière, E. 1987, *Astr. Ap.*, **187**, 761.
Lentz, W. J. 1976, *Appl. Optics*, **15**, 668.
Levasseur-Regourd, A. C., and Dumont, R. 1986, *Adv. Space Res.*, **6**, 87.
Lewis, R. S., Ming, T., Wacker, J. R., Anders E., and Steel, E. 1987, *Nature*, **326**, 160.
Lienert, C., Richter, I., Pitz, E., and Planck, N. 1981, *Astr. Ap.*, **103**, 177.
Martin, P. G., and Rogers, C. 1987, *Ap. J.*, **322**, 374.
Maurette, M., Jéhanno, C., Robin, G., and Hammer, C. 1987, *Nature*, **328**, 699.
Mazets, E. P., *et al.* 1986, in *20th ESLAB Symposium* (ESA SP-250, Vol. **2**, p. 3).
McDonnell, J. A. M., *et al.* 1987, *Astr. Ap.*, **187**, 719.
Mukai, T., Mukai, S., and Kikuchi, S. 1987, *Astr. Ap.*, **187**, 650.
Murdock, T. L., and Price, S. D. 1985, *A.J.*, **90**, 375.
Phillip, H. R. 1977, *Phys. Rev. B*, **16**, 2896.
Pollack, J. B., Toon, O. B., and Khare, B. N. 1973, *Icarus*, **19**, 372.
Reach, W. T. 1988, in preparation (Paper II).
Reach, W. T., and Heiles, C. 1988, in *Proc. Third Internat. IRAS Conf., Comets to Cosmology*, ed. A. Lawrence (Lecture Notes in Physics; Berlin: Springer-Verlag), p. 40.
Röser, S., and Staude, H. J. 1978, *Astr. Ap.*, **67**, 381.
Salama, A. *et al.* 1987, *A.J.*, **92**, 467.
Sandford, S. A., and Walker, R. M. 1985, *Ap. J.*, **291**, 838.
Taft, E. A., and Phillip, H. R. 1965, *Phys. Rev.*, **138**, A197.
Toon, O. B., and Ackerman, T. P. 1981, *Appl. Optics*, **20**, 3657.
van de Hulst, H. C. 1957, *Light Scattering by Small Particles* (New York: Wiley).
Wiscombe, W. J. 1980, *Appl. Optics*, **19**, 1505.
Wright, E. W. 1987, *Ap. J.*, **320**, 818.
Zook, H. A., Lange, G., Grún, E., and Fechtig, H. 1984, *Lunar Planet Sci.*, **15**, 965.

WILLIAM T. REACH: Astronomy Department, University of California, Berkeley, CA 94720